Slot Filling Factor Calculation and Electromagnetic Performance of Single Phase Electrically Excited Flux Switching Motors

Bakhtiar Khan, Faisal Khan, Wasiq Ullah, Muhammad Umair, and Shahid Hussain

Department of Electrical & Computer Engineering
COMSATS University Islamabad, Abbottabad Campus, Pakistan
engr.bakhtiarkhan@gmail.com

Abstract — For variable speed applications, flux controlling capability of electrically excited flux switching motors (EEFSMs) attract researchers' attention. However, low copper slot filling factor of the EEFSM with standard stator slot vitiates the electromagnetic performance and efficiency. This paper has proposed a new Octane Modular Stator (OMS) EEFSM model that has pentagonal stator slot and high copper slot filling factor. Copper slot filling factor is deliberated analytically for the proposed model and designs with standard stator slots, i.e., trapezoidal and rectangular. Electromagnetic performance of the OMS, Rectangular Stator Slot (RSS) and Trapezoidal Stator Slot (TSS) EEFSM designs are evaluated by finite element analysis (FEA) through JMAG v18.1 FEA solver. The proposed OMS EEFSM model has 9% higher copper slot filling factor in comparison with standard stator slots designs under same geometric parameters. The high copper slot filling factor of the proposed OMS EEFSM model has improved performance in term of low electric and magnetic loading.

Index Terms — Electrically Excited Flux Switching Motor (EEFSM), Finite Element Analysis (FEA), non-overlapped windings, Octane Modular Stator (OMS), single phase motor, salient rotor.

I. INTRODUCTION

Strong overload capability, high average torque, low torque ripples and high efficiency are the main desired characteristics of every motor and especially for high speed applications [1-4]. In permanent magnet (PM) flux switching motor (FSM), PM as well as armature windings are located at stator and making a robust rotor structure. Furthermore, it has high power density, easy heat dissipation and suitable for high speed applications. Despite these pros, in this type FSM an enormous amount of rare earth permanent magnet is used that overall increases the cost of the machine. The resources of the PM material are depleting day by day and prices to be raised [5-9]. As temperature suddenly increases the performance of the PMFSM is greatly degraded and

hence limiting its application at high temperature. The fixed and uncontrolled flux is the undesired characteristic for variable high speed operations [10-11]. The flux of electrically excited (EE) FSM can be controlled electronically, performance is not degraded with increase in temperature and overall cost is low. The simple manufacturing process of single phase EEFSM, easy maintenance, longer lifetime and low cost are the core points that prioritized it for high speed applications [12].

For fan applications, single phase 12Slots-6Poles (12S-6P) EEFSM novel design with trapezoidal slot stator, non-overlapped windings arrangement and segmental rotor has presented in [13]. The key characteristics of this design are low weight, less copper losses and higher efficiency. However, it cannot be used for high speed operations as it has segmental rotor. In [14] authors have presented two novel model 12S-6P and 8S-4P designs of single phase EEFSM with overlapped windings arrangement and both the designs are validated experimentally. In these design overlapped windings arrangement cause high copper losses. Authors have designed a novel model 8S-6P single phase EEFSM with non-overlapped windings arrangement in [15], this design has robust rotor structure and low copper losses. Similarly 24S-10P single phase EEFSM is proposed in [16]. All the designs discussed above have standard trapezoidal slot structure. High power density and efficiency are key factors for motors used in high speed applications. The most desired characteristics for high speed operation are high power density and high efficiency [17-18]. Increasing copper slot filling factor of the stator windings of EEFSM can increase the power density and efficiency [19]. This work has proposed single phase 8S-6P Octane Modular Stator (OMS) EEFSM model and the direction for this design is from [20] as presented by Fig. 1. The proposed model has pentagonal slot structure which has high copper slot filling factor than the trapezoidal stator slot (TSS) and rectangular stator slot (RSS), and this is validated via algorithm [21]. Design methodology, copper slot filling factor calculation, no-load analysis, load analysis and

conclusion are conferred in Sections II, III, IV, V and VI respectively.

Fig. 1. Poki-Poki model of MITSUBISHI ELECTRIC.

II. DESIGN METHODOLOGY

The three single phase 8S-6P topologies shown in Fig. 2 are designed and analyzed in JMAG v18.1 as per geometric design parameters given in Table 1. The position of the field/armature windings are justified through coils arrangement test.
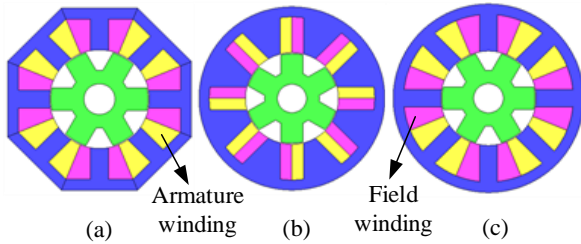
Fig. 2. Electrically excited FSMs: (a) OMS, (b) RSS, and (c) TSS.

Table 1: Single phase 8S-6P EEFSMs parameters

Design Parameter	OMS	TSS	RSS
Stator slot width (mm)	8.2		
Stator yoke height (mm)	5		
Field/armature slots area (mm^2)	430.08	607.12	401.44
Stator outer radius (mm)	45		
Armature/field coil turns	154	180	129
Armature current (A) @ 15A/mm^2	6.57	6.73	6.60
Field excitation current (A) @ 15A/mm^2	4.65	4.75	4.67

III. COPPER SLOT FILLING FACTOR CALCULATION

Copper slot filling factor is calculated by procedure in [21] for the OMS, RSS, TSS EEFSM designs and the results are compared. The input parameters of the algorithm are the slot cross section and dimensions of the wire, where the output is the highest figure of conductors in the slot to be accommodated. Equation (1) is mathematical model for the copper slot filling factor:

$$f_{slot} = \frac{N_w \times A_w}{A_{slot}}. \tag{1}$$

Here f_{slot} is copper slot filling factor, N_w number of copper conductors, A_w cross-sectional area of conductor and A_{slot} slot area. As the copper losses are inversely proportional to copper cross section, so maximizing the copper slot filling factor will minimize the copper losses. Below in Fig. 3 are the slot sections of OMS, TSS and RSS EEFSMs.
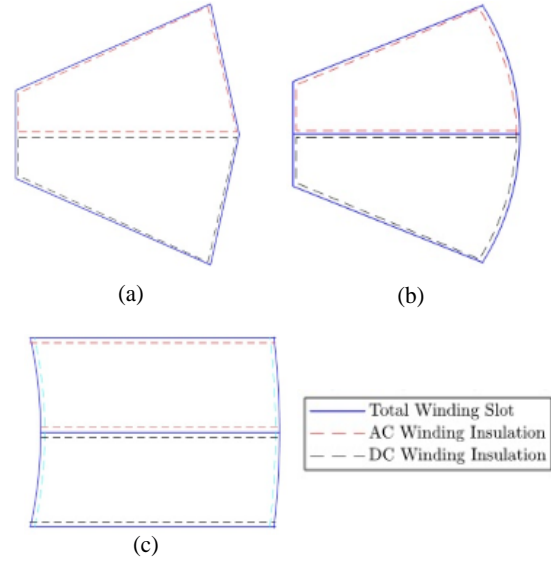
Fig. 3. Slot sections of EEFSM: (a) OMS, (b) TSS, and (c) RSS.

The algorithm for this work has been implemented in MATLAB and geometrical model of the slots are used. Also it is important to select the dimensions and type of the conductor. To insert a conductor in the slot, the conditions below to be satisfied. Here (x_c, y_c) and d_{max} represent the center point and diameter of the circular conductor. The distance of the conductor from y-axis is d_1, x-axis d_2, slop line d_3 and arc d_4 as in Fig. 4. For any conductor to be inside the slot profile, the conditions applied in *xy* frame reference are:

for $d_1 \geq 0$;

$$|(x_c - d_{max}/2) - x_{vline}| \geq 0. \tag{2}$$

for $d_2 \geq 0$;

$$|(y_c - d_{max}/2) - y_{hline}| \geq 0. \tag{3}$$

for $d_3 \geq 0$;
  if $y_c > 0$;

$$\frac{(y_{pline} - y_c) - s_{line} \cdot (x_{pline} - x_c)}{\sqrt{s^2_{line} + 1}} - \frac{d_{max}}{2} \geq 0. \tag{4}$$

  if $y_c < 0$;

$$\frac{(y_{pline} + y_c) - s_{line} \cdot (x_{pline} - x_c)}{\sqrt{s^2_{line} + 1}} - \frac{d_{max}}{2} \geq 0. \tag{5}$$

$for\ d_4 \geq 0;$
$if\ y_c > 0;$

$$\left(r_{1,2} - \frac{d_{max}}{2}\right) - \sqrt{\left(x_c - x_{c,arc}\right)^2 + \left(y_c - y_{c,arc}\right)^2} \geq 0. \quad (6)$$

$if\ y_c < 0;$

$$\left(r_{1,2} - \frac{d_{max}}{2}\right) - \sqrt{\left(x_c - x_{c,arc}\right)^2 + \left(y_{c,arc} - y_c\right)^2} \geq 0. \quad (7)$$
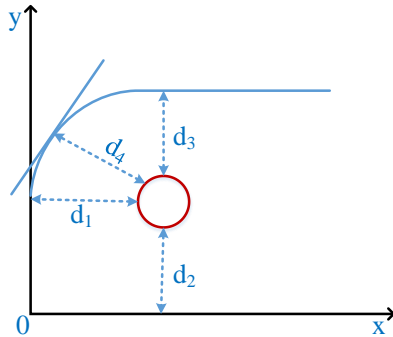
Fig. 4. Conductor placement in slot.

Figure 3 shows the horizontal implementation of slot contour in algorithm. Before starting the algorithm, the placement of first conductor is the first step and coordinate for its center are:

$$x_c = \frac{d_{max}}{2} + d + x_i\ ;\ \ y_c = -\left(\frac{w + d_{max}}{2}\right) + y_i. \quad (8)$$

For placement the conductors in the remaining part of slot, the slot area is divided into grid of i_{th} columns and j_{th} rows. Circular conductors are always placed in honey comb structure. Equations (9) and (10) are used to determine the maximum number of rows and columns:

$$i_{max} = round\left(\frac{x_E}{\sqrt{3d_{max}/2}}\right), \quad (9)$$

$$j_{max} = round\left(\frac{w}{d_{max}}\right). \quad (10)$$

Round(x) rounds each element of x to nearest integer. Two "for loops" are used here, the outer loop fixes the index i and inner loop varying index j:

$$y_c(i, j + 1) = y_c(i, j) + d_{max} + d_w. \quad (11)$$

After the increment in index i, conductor center coordinates are given by equations (12) and (13):

$$x_c(i + 1, j) = x_c(i, j) + \sqrt{3/2} \cdot (d_{max} + d_w), \quad (12)$$

$$y_c(i + 1, j) = y_c(i, j) + mod(i + 1, 2) \cdot d_{max}/2. \quad (13)$$

Where mod(i+1, 2) is a function that returns the module after division between 'i+1' and 2. The results of the algorithm implemented in MATLAB for the arrangement

of conductors in slots are in Fig. 5. The dimensions of the conductors in all three designs are selected according to maximum current requirement for the field and armature windings. Copper slot filling factor for each type slot is calculated by the mathematical model (1), results are presented in Fig. 6 and tabulated in Table 2. From the results it can be seen, the copper slot filling factor of OMS slot is 7% higher than that of TSS and 9% higher than that of RSS.
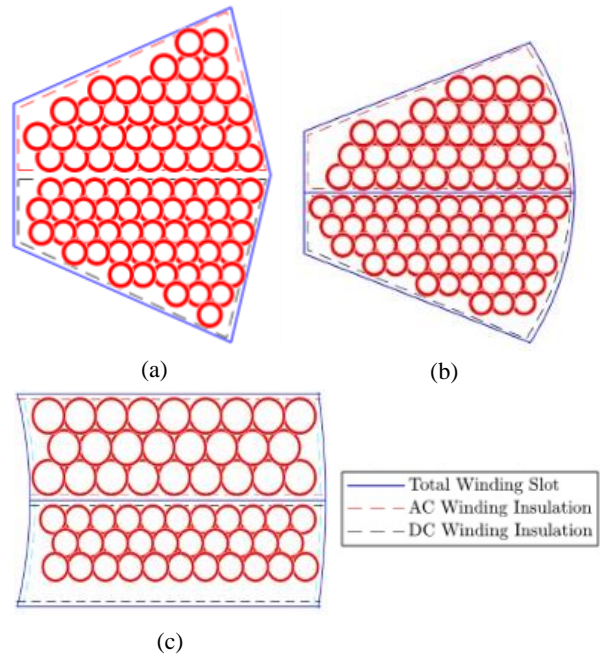
Fig. 5. MATLAB results for copper slot filling: (a) OMS, (b) TSS, and (c) RSS.
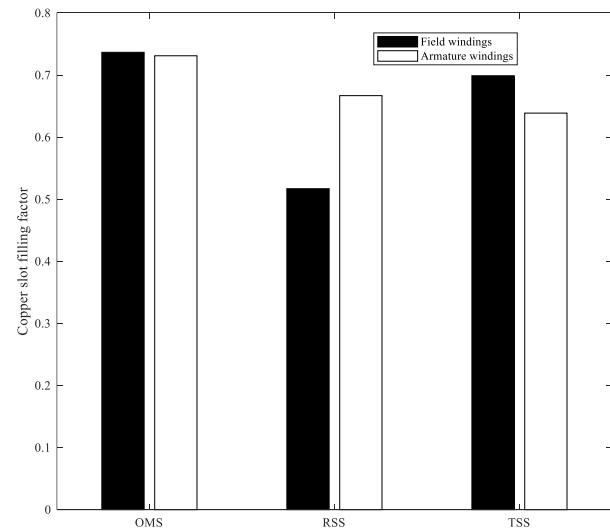
Fig. 6. Comparison of copper slot filling factor for three designs.

Table 2: Single phase 8S-6P EEFSMs copper slot filling factor

Description	Copper Slot Filling Factor		
	OMS	TSS	RSS
Field slot	0.73661	0.69890	0.51686
Armature slot	0.73103	0.63867	0.66682

IV. NO-LOAD ANALYSIS

The no-load analysis key indicators are: flux linkage, cogging torque, back-emf and total harmonic distortion (THD), all these are discussed in subsections.

A. Flux linkage

The operation of single phase 8S-6P OMS, TSS and RSS EEFSMs for non-overlapped windings arrangement is validated via coil test. Equations (14) and (15) are used to calculate the EE coil current density J_e and armature coil current density J_a. For the three designs no-load magnetic flux linkage are analyzed and compared, the EE windings current density is set to 15A/mm^2 and the results are presented in Fig. 7. TSS machine design has the highest flux linkage of 0.069Wb, where OMS has 0.050Wb and RSS design has the lowest 0.029Wb at maximum J_e=15A/mm^2 and J_a=0:

$$J_a = \frac{I_a N_a}{S_a \alpha_a}, \qquad (14)$$

$$J_e = \frac{I_e N_e}{S_e \alpha_e}. \qquad (15)$$

Where, J, S, N, and α represents current-density, slot-area, number of turns, and winding-factor respectively while subscripts "a" and "e" represent armature and EE coils correspondingly.
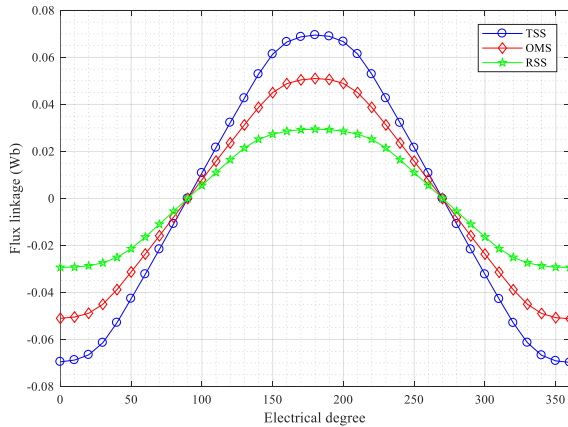
Fig. 7. No-load flux linkage.

B. Cogging torque

The J_e =15A/mm^2 current density of EE coil, J_a=0 armature coil current density and 1000 rpm rotor speed are used for the no-load cogging torque analysis at different rotor position represented by mechanical degree. Figure 8 shows cogging torque comparison of three designs which illustrates that RSS EEFSM design has lowest maximum peak cogging torque value of 0.010Nm as compared to the other designs of this paper. Where TSS has the highest maximum peak cogging torque of 0.136Nm and OMS model has the maximum peak cogging torque value of 0.10Nm.
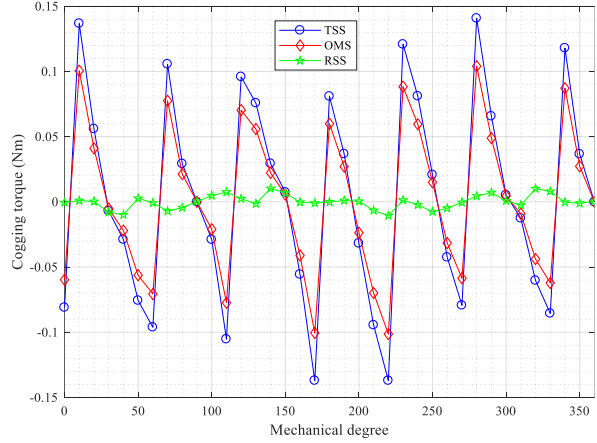
Fig. 8. Single phase no-load cogging torque.

C. Back-emf

2D FEM is used for the investigation of no-load back emf and the designs discussed above are included in this analysis. The no-load parameters were kept the same, i.e., J_e =15A/mm^2 current density of EE coil, J_a=0 armature coil current density and 1000 rpm rotor speed for all no-load tests. The results of the no-load back emf versus rotor position in electrical degree are presented in Fig. 9. In this study, TSS EEFSM design has the highest maximum peak back emf of 39.124 volts, where that of OMS is 28.711 volts. RSS design has the lowest maximum peak back emf value of 1.976 volts but back emf maximum peak values of all three designs are in the range of normal operation and graphs pattern is identical at different field currents.

D. Total harmonic distortion

The performance of conductors and insulators of electrical machines are degraded by harmonics, therefore, the calculation of total harmonic distortion (THD) for the all three designs are obligatory and obtained via equation (16):

$$THD = \frac{\sqrt{3_{rd}harmonic^2 + 5_{th}harmonic^2 + 7_{th}harmonic^2 + \cdots}}{1_{st}\ harmonic}. \qquad (16)$$

The calculated THDs from the simulation results are: RSS 8S-6P single phase EEFSM design has the highest THD vale of 4.465%, TSS and OMS models have almost the same THD values of 3%. For better performance and

long lifetime of electrical machines, the THD should be always less than 5%.
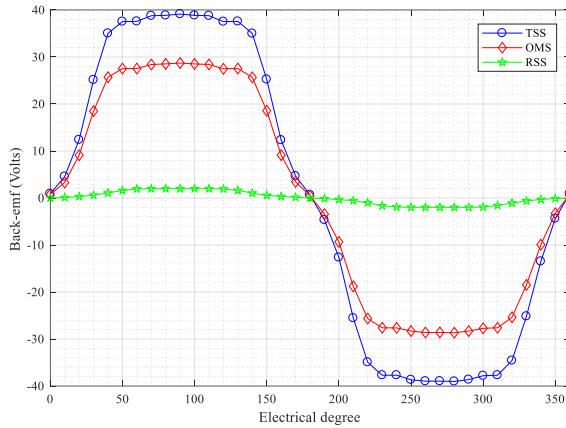
Fig. 9. No-load back-emf.

V. LOAD ANALYSIS

This section comprises analysis of average torque, instantaneous torque, torque and output power versus speed, losses and efficiency. Each one are deliberated in detail in the following subsections.

A. Average torque

The average-torque of single phase 8S-6P OMS, TSS and RSS EEFSM with salient rotor designs are shown in Fig. 10. The current density of EE coil is kept constant at $J_e=15$A/mm^2 and armature current-density J_a range is varied from 2.5A/mm^2 to 15A/mm^2. From 2D FEM analysis it is observed that increase in armature current density changing the average electromagnetic torque proportionally. TSS design with non-overlapped windings arrangement has the highest average electromagnetic torque value of 0.85 Nm, OMS has average electromagnetic torque 0.77 Nm and RSS has the lowest average electromagnetic torque value 0.58 Nm.
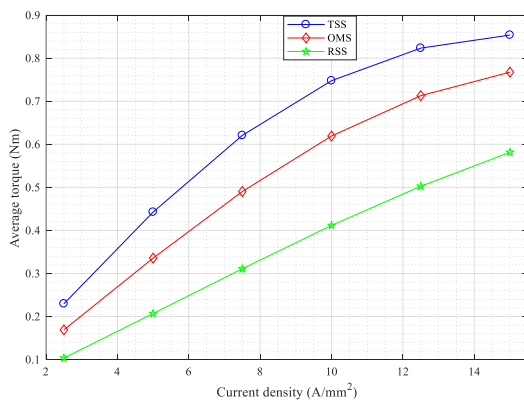
Fig. 10. Average torque vs J_a at $J_e=15$A/mm^2 plot.

B. Instantaneous torque

Instantaneous torque is the important part of load analysis, simulation results of the 2D FEA for the instantaneous torque at various rotor positions in electrical degree are labeled by different lines in Fig. 11 for the three designs. The TSS model has the highest maximum peak instantaneous torque value of 1.86 Nm and minimum bottom value -0.138 Nm. OMS EEFSM has maximum peak instantaneous torque value of 1.55 Nm and minimum bottom value -0.109 Nm, where RSS design has the lowest maximum peak value of 1.28 Nm and minimum bottom value -0.00002 Nm. This shows that TSS design has the highest peak to peak ripples, RSS design has the lowest and OMS has peak to peak ripples in-between the other two designs.
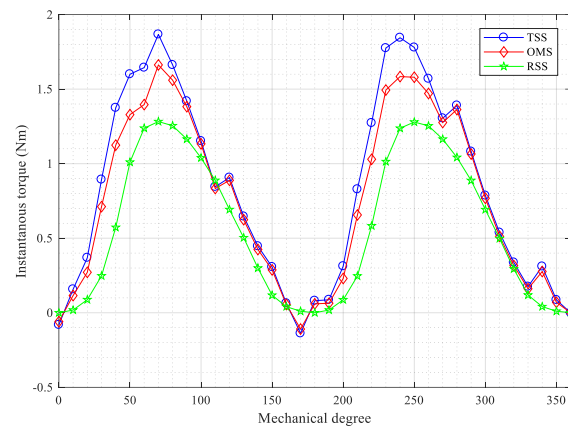
Fig. 11. Instantaneous torque.

C. Average torque and output power versus speed

The torque and power versus speed curves of the initial designs of the EEFSM are plotted in Fig. 12. The maximum torque of OMS, TSS and RSS are 0.83 Nm, 0.94 Nm and 0.59 Nm at speed 1327.5 rpm, 1036.3 rpm and 1913.3 rpm respectively. Similarly, the maximum output power of the above discussed designs are 115.42 watt, 109.5 watt and 119.75 watt at speed 1327.5 rpm, 1362.2 rpm and 1913.3. Below and above these speeds the average torque and output power are reduced. Analysis of the deliberated three EEFSMs show that OMS EEFSM has stable and high average torque and output power at same speed, while for the other two designs either average torque or output power are low. So, OMS EEFSM is the suitable option out of the three designs.

D. Losses and efficiency analysis

Core losses for the three designs are assessed by 2D-FEA via JMAG v18.1 FEA solver, while copper losses are calculated by the following equation [22]:

$$P_c = \rho(2L + 2L_{end}) \times J \times I \times N \times n_{slot}. \qquad (17)$$

In (17) P_c copper losses, $\rho = 2.224 \times 10^{-8} \Omega m$ copper resistivity, L stack length, L_{end} calculated end coil length, J current density, I current, N number of turns and n_{slot} number of pairs of slots. OMS-EEFSM has efficiency 76.7% and losses 37.7 watt, the efficiency of TSS-EEFSM is 66.6% and losses are 60.64 watt and RSS-EEFSM has 75.3% efficiency and 34.37 watt losses.
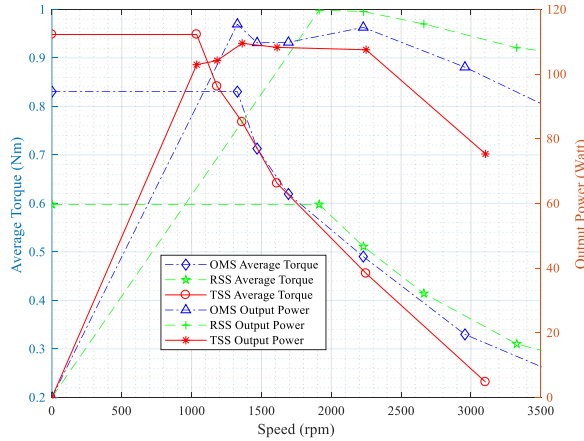
Fig. 12. Average torque and output power vs speed.

VI. CONCLUSION

Single phase OMS 8S-6P, TSS and RSS EEFSM with salient rotor are designed and evaluated in this research work. Copper slot filling factor is calculated for the three designs, the proposed design OMS model has 7% higher copper slot filling factor than TSS design and 9% higher than the RSS with the same geometric specifications, which is the core motive of this work. No-load and load analysis are carried out, the average torque of the proposed un-optimized OMS EEFSM model is 0.90 times of TSS design, at the cost of 17% less number of field and armature windings turns, 3% less field current and 3% less armature current. Besides, the peak to peak value of the instantaneous torque for the proposed design is 20% less than the TSS design, this entails that the proposed design has less peak to peak ripples than the standard trapezoidal slot design. Copper losses OMS EEFSM are 0.62 times that of TSS EEFSM and 1.09 times that of RSS EEFSM. Similarly, efficiency of proposed model is 1.15 times that TSS EEFSM and 1.02 times that of RSS EEFSM. Although the copper losses of RSS EEFSM are less than OMS EEFSM but OMS EEFSM has 1.4 times high average torque than RSS EEFSM and 0.90 times that of TSS EEFSM at the same current density. Based on the analysis, it is concluded that the proposed OMS EEFSM model has better overall performance, copper losses can be reduced, average torque and efficiency of the initial design can be further improved by optimization and is best option for high speed applications.

REFERENCES

[1] P. Su, W. Hua, M. Hu, Z. Wu, J. Si, Z. Chen, and M. Cheng, "Analysis of stator slots and rotor pole pairs combinations of rotor-permanent magnet flux-switching machines," *IEEE Trans. Ind. Electron.*, vol. 67, no. 2, pp. 906-918, 2019.

[2] N. Ullah, M. K. Khan, F. Khan, A. Basit, W. Ullah, T. Ahmad, and N. Ahmad, "Comparison of analytical methodologies for analysis of single sided linear permanent magnet flux switching machine: No-load operation," *ACES Journal*, vol. 33, no. 8, pp. 923-930, 2018.

[3] N. Ahmad, F. Khan, N. Ullah, and M. Z. Ahmad "Performance analysis of outer rotor wound field flux switching machine for direct drive application," *ACES Journal*, vol. 33, no. 8, pp. 913-922, 2018.

[4] M. M. Nezamabadi, E. Afjei, and H. Torkama, "Design and electromagnetic analysis of a new rotary-linear switched reluctance motor in static mode," *ACES Journal*, vol. 31, no. 2, pp. 171-179, 2016.

[5] Z. Q. Zhu and J. T. Chen, "Advanced flux-switching permanent magnet brushless machines," *IEEE Trans. Magn.*, vol. 46, no. 6, pp. 1447-1453, June 2010.

[6] X. Zhu, Z. Shu, L. Quan, Z. Xiang, and X. Pan, "Design and multicondition comparison of two outer-rotor flux-switching permanent magnet motors for in-wheel traction applications," *IEEE Trans. Ind. Electron.*, vol. 64, no. 8, pp. 6137-6148, Aug. 2017.

[7] H. Yang, H. Lin, Z. Q. Zhu, D. Wang, S. Fang, and Y. Huang, "A variable-flux hybrid-PM switched-flux memory machine for EV/HEV applications," *IEEE Trans. Ind. Appl.*, vol. 52, no. 3, pp. 2203-2214, May/June 2016.

[8] Z. Xiang, X. Zhu, L. Quan, and D. Fan, "Optimization design and analysis of a hybrid permanent magnet flux-switching motor with compound rotor configuration," *CES Trans. Electrical Machines and Systems*, vol. 2, no. 2, pp. 200-206, 2018.

[9] Z. Z. Wu and Z. Q. Zhu, "Analysis of air-gap field modulation and magnetic gearing effects in switched flux permanent magnet machines," *IEEE Trans. Magnetics*, vol. 51, no. 5, pp. 1-12, 2015.

[10] F. Khan, E. Sulaiman, and M. Z. Ahmad, "Review of switched flux wound-field machines technology," *IETE Technical Review*, vol. 34, no. 4, pp. 343-352, 2017.

[11] E. Sulaiman, T. Kosaka, and N. Matsui, "High power density design of 6-slot–8-pole hybrid excitation flux switching machine for hybrid electric vehicles," *IEEE Trans. Magnetics*, vol. 47, no. 10, pp. 4453-4456, 2011.

[12] E. Sulaiman, M. F. M. Teridi, Z. A. Husin, M. Z. Ahmad, and T. Kosaka, "Performance comparison of 24S-10P and 24S-14P field excitation flux switching machine with single DC-Coil polarity," *7th International Power Engineering and Optimization Conference (PEOCO), IEEE*, pp. 46-51, 2013.

[13] M. F. Omar, E. Sulaiman, M. Jenal, R. Kumar, and R. N. Firdaus, "Magnetic flux analysis of a new field-excitation flux switching motor using segmental rotor," *IEEE Trans. Magnetics*, vol. 53, no. 11, pp. 1-4, 2017.

[14] Y. J. Zhou and Z. Q. Zhu, "Comparison of low-cost single-phase wound-field switched-flux machines," *IEEE Trans. Ind. Appl.*, vol. 50, no. 5, pp. 3335-3345, 2014.

[15] S. Ishaq, F. Khan, N. Ahmad, K. Ayaz, and W. Ullah, "Analytical modeling of low cost single phase wound field flux switching machine," *1st International Conference on Power, Energy and Smart Grid (ICPESG), IEEE*, pp. 1-6, 2018.

[16] J. Yuan, D. Meng, G. Lian, J. Zhang, H. Li, and F. Ban, "The stator slot-type optimization of electrical excitation flux-switching motor and its maximum torque/copper loss control," *IEEE Trans. Appl. Supercond.*, vol. 29, no. 2, pp. 1-5, 2019.

[17] G. Zhao, W. Hua, and J. Qi, "Comparative study of wound-field flux-switching machines and switched reluctance machines," *IEEE Trans. Ind. Appl.*, vol. 55, no. 3, pp. 2581-2591, 2019.

[18] H. J. Park and M. S. Lim, "Design of high power density and high efficiency wound-field synchronous motor for electric vehicle traction," *IEEE Access*, vol. 7, pp. 46677-46685, 2019.

[19] P. Herrmann, P. Stenzel, U. Vogele, and C. Endisch, "Optimization algorithms for maximizing the slot filling factor of technically feasible slot geometries and winding layouts," *6th International Electric Drives Production Conference (EDPC), IEEE*, pp. 149-155, 2016.

[20] T. Komatsu and A. Daikoku, "Elevator traction-machine motors," *Motor Technologies for Industry and Daily Life Edition*, 2003.

[21] A. O. D. Tommaso, F. Genduso, R. Miceli, and C. Nevoloso, "Fast procedure for the calculation of maximum slot filling factors in electrical machines," *12th International Conference on Ecological Vehicles and Renewable Energies (EVER), IEEE*, pp. 1-8, 2017.

[22] F. Khan, E. Sulaiman, and M. Z. Ahmad, "A novel wound field flux switching machine with salient pole rotor and nonoverlapping windings," *Turkish Journal of Electrical Engineering & Computer Sciences*, vol. 25, pp. 950-964, 2017.

Bakhtiar Khan received his B.Sc. and M.Sc. degree in Electrical Engineering from University of Engineering & Technology, Peshawar Pakistan and COMSATS University Islamabad (CUI), Abbottabad Campus, Pakistan in 2007 and 2018 respectively. He is currently enrolled in Ph.D. Electrical Engineering at CUI Abbottabad. His research interest includes design and analysis of electrical machines.

Faisal Khan received his Ph.D. degree in Electrical Engineering from Universiti Tun Hussien Onn Malaysia in 2016. Currently he is working as Assistant Professor at CUI, Abbottabad Campus.
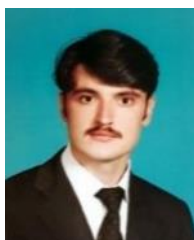
Wasiq Ullah received his B.S. degree in Electrical Engineering from CUI, Abbottabad Campus, Pakisan in 2018 and is currently enrolled in M.S. Electrical Engineering at CUI, Abbottabad Campus, Pakistan. He is research member of Electrical Machine Design Group.

Muhammad Umair received his B.S. degree in Electrical Engineering from CUI, Abbottabad Campus, Pakisan in 2018 and is currently enrolled in M.S. Electrical Engineering at CUI, Abbottabad Campus, Pakistan. He is working as Research Assistant in the Department of Electrical and Computer Engineering CUI, Abbottabad Campus, Pakistan. He is also research member of Electrical Machine Design Group.

Shahid Hussain has completed his B.S. Electrical Engineering degree in July, 2019 from CUI, Abbottabad Campus. He is Research Member of Electrical Machine Design Group.